

Globular clusters: absolute proper motions and Galactic orbits

A. A. Chemel',¹ E. V. Glushkova,^{2,1,*} A. K. Dambis,^{3,†}
A. S. Rastorguev,^{2,1,‡} L. N. Yalyalieva,^{2,1} and A. D. Klinichev¹

¹*Lomonosov Moscow State University, Faculty of Physics,
1, bld.2, Leninskie Gory, Moscow, 119992, Russia*

²*Sternberg Astronomical Institute, 13, Universitetskii prospect, Moscow, 119992, Russia*

³*Sternberg Astronomical Institute, Lomonosov Moscow State University,
13, Universitetskii prospect, Moscow, 119992, Russia*

We cross-match objects from several different astronomical catalogs to determine the absolute proper motions of stars within the 30-arcmin radius fields of 115 Milky-Way globular clusters with the accuracy of 1–2 mas/yr. The proper motions are based on positional data recovered from the USNO-B1, 2MASS, URAT1, ALLWISE, UCAC5, and GAIA DR1 surveys with up to 10 positions spanning an epoch difference of up to ~ 65 years, and reduced to GAIA DR1 TGAS frame using UCAC5 as the reference catalog. Cluster members are photometrically identified by selecting horizontal- and red-giant branch stars on color-magnitude diagrams, and the mean absolute proper motions of the clusters with a typical formal error of ~ 0.4 mas/yr are computed by averaging the proper motions of selected members. The inferred absolute proper motions of clusters are combined with available radial-velocity data and heliocentric distance estimates to compute the cluster orbits in terms of the Galactic potential models based on Miyamoto and Nagai disk, Hernquist spheroid, and modified isothermal dark-matter halo (axisymmetric model without a bar) and the same model + rotating Ferre's bar (non-axisymmetric). Five distant clusters have higher-than-escape velocities, most likely due to large errors of computed transversal velocities, whereas the computed orbits of all other clusters remain bound to the Galaxy. Unlike previously published results, we find the bar to affect substantially the orbits of most of the clusters, even those at large Galactocentric distances, bringing appreciable chaotization, especially in the portions of the orbits close to the Galactic center, and stretching out the orbits of some of the thick-disk clusters.

I. INTRODUCTION

Globular clusters (GCs) are potentially very important tracers of the kinematics of the Galactic bulge and halo from the inner parts of the Galaxy to its distant outskirts. Despite their scarcity (about 150 objects) globular clusters have a number of important advantages over other, more populous halo probes (e.g. RR Lyrae-type variables and blue horizontal branch stars): the sample of currently catalogued GCs [23] is much more complete than the corresponding samples of RR Lyrae variables and blue horizontal branch stars, and due to the group nature of GCs their inferred parameters (e.g., heliocentric distances, heavy-element abundances and radial velocities) are much more accurate and reliable than those of individual stars. Unlike the situation with the space distribution of the GC population, which is known rather accurately, the kinematical picture of this population remains incomplete in that we have to rely only on its one-dimensional projection with only one velocity component – the line-of-sight velocity – currently known more or less accurately for most of the clusters. The absolute proper-motion data for GCs [4–8, 12–17, 24, 27, 29, 30, 33, 37, 38, 42] still remains rather incomplete, not very accurate, or controversial.

In this paper we use the UCAC5[40] catalog, whose reference frame is based on GAIA TGAS catalog[31], and combine it with a number of all-sky and large-scale sky surveys (USNO-B1.0 [32], 2MASS [35], URAT1 citeURAT, WISE [28, 39], and Gaia [18]) released in the last couple of decades and based on observations acquired in ~ 1950 –2015 in an attempt to estimate the absolute proper motions of stars in the GC neighborhood, identify likely cluster members, and determine the average proper motions for most of the catalogued GCs. To provisionally validate our results, we estimate the average velocity components and the velocity dispersion components for the subsample of metal-poor GCs ($[Fe/H] < -1.0$) and compute Galactic orbits for all clusters of our sample.

II. DATA AND TECHNIQUE

Our aim is to compute the absolute proper motions of stars in the fields of globular clusters, identify the likely cluster members, and compute the mean proper motions of the clusters studied by averaging the inferred proper motions for selected cluster members.

We begin by estimating the proper motions of most of the stars in the fields of cluster considered based on the star positions recovered from a number of the most extensive sky surveys (USNO-B1.0, 2MASS, WISE, URAT1, UCAC5, GAIA DR1) containing good positional data.

The first step is to cross-match stars from these surveys in the cluster fields. To facilitate this task, we

*Electronic address: elena.glushkova@gmail.com

†Electronic address: dambis@yandex.ru

‡Electronic address: alex.rastorguev@gmail.com

developed a command-line CROSSMATCH program [25] written in java programming language and serving as a convenient interface to the well-known STILTS program [36]. CROSSMATCH code is available at www.sai.msu.ru/groups/cluster/cl/crossmatch/Crossmatch_4.3.0.zip

For each cluster we begin our analysis by cross-matching stars from the above catalogs within 30 arcmin of the cluster centers with a cross-match radius of 1 or 2 arcsec.

The next step is to bring the positions adopted from the survey catalogs to the frame defined by Gaia DR1 positions and proper motions. The problem is that although bona fide 2015.0 positions are currently available for more than 1 billion Gaia stars, Gaia proper motions are available only for > 2 million stars of the Gaia TGAS subset [31], which is evidently insufficient for proper astrometric reduction in cluster fields for two reasons:

1. The subset is insufficiently dense to provide enough stars per field
2. The subset consists of too bright stars, whose images are too saturated in the surveys considered and therefore their measured positions are fraught with systematic errors and cannot be used to determine reduction parameters for fainter stars.

To overcome this difficulty, we use the much deeper and more extensive UCAC5 catalogue [40] as our reference set instead of Gaia FR1 TGAS. According to its authors, UCAC5 should be a good extension of Gaia DR1 TGAS down to limiting magnitudes of $\sim 16.0^m$ and fainter. We therefore adopt UCAC5 positions as is without applying any corrections. Naturally, we treat published Gaia 2015.0 positions in the same way. We bring the WISE MJD=55400.0 (2010.5589) positions to UCAC5 frame via usual linear plate adjustment and do the same with 2MASS and URAT1 positions. As for USNO-B10, we reconstruct the positions of the star's images on individual Schmidt plates based on the information provided in the USNO-B1.0 Catalog [32] (the J2000.0 position, proper motion, and tangent-plane offsets — $B1_\xi$, $B2_\xi$, $R1_\xi$, $R2_\xi$, I_ξ and $B1_\eta$, $B2_\eta$, $R1_\eta$, $R2_\eta$, I_η — along the x- and y-directions with respect to the mean-epoch position). Again, we perform linear plate adjustment using UCAC5 stars located within 30 arcmin of the cluster centre as reference objects and adopting individual USNO-B1.0 plate epochs from plate logs at the page

<http://www.nofs.navy.mil/data/fchpix/cfhelp.html#plogs> of the site of USNO Flagstaff Station Integrated Image and Catalogue Archive Service (see [9]). As a result, we obtain a maximum of ten positions (a maximum of five reconstructed Schmidt plate positions from USNO-B1.0 + Gaia position + one UCAC5 position+ one reconstructed position from each of the 2MASS, URAT1, and ALLWISE catalogs per star north of $\delta = -33.0^\circ$, and a maximum of three reconstructed Schmidt plate

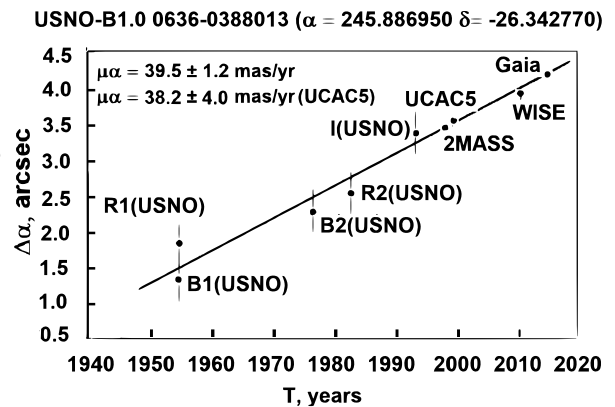


FIG. 1: Right ascension difference for star USNO-B1.0 0636-0388013 as a function of epoch. The dots with errorbars show the reconstructed positions in the UCAC5 reference frame. The solid line shows the linear least squares fit used to determine the proper motion.

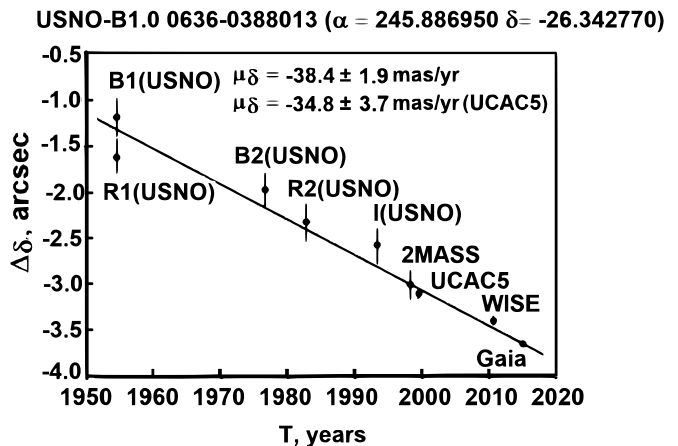


FIG. 2: Declination difference for star USNO-B1.0 0636-0388013 as a function of epoch. The dots with errorbars show the reconstructed positions in the UCAC5 reference frame. The solid line shows the linear least squares fit used to determine the proper motion.

positions from USNO-B1.0 + Gaia position + one UCAC5 position+ one reconstructed position from each of the 2MASS and ALLWISE catalogs per star south of $\delta = -33.0^\circ$). The total epoch span usually varies from about 65 years for stars north of $\delta = -33.0^\circ$ to about 30–35 years for stars south of $\delta = -33.0^\circ$.

To illustrate the procedure, we show in Figs. 1 and 2 the variation of the right ascension and declination, respectively, of the star USNO-B1.0 0636-0388013 as a function of epoch. The dots with the errorbars show the corresponding reconstructed positions and the solid lines, the linear least squares fit used to determine the proper motion. As is evident from the figures, the use of extra positional data improves appreciably the accuracy of the proper-motion components compared to UCAC5.

We then identify the likely cluster members by selecting stars from the horizontal and red-giant branches

and the main sequence in the cluster color-magnitude diagrams based on 2MASS data and compute the average proper-motion components along right ascension and declination.

To validate our technique, we also determine the proper motions of nearby globular clusters (i.e., those whose horizontal- and red-giant branch stars are well within the UCAC5 limiting magnitude) based on the original UCAC5 proper motions of the cluster members, and compare the results with those obtained for fainter, main-sequence stars of the cluster determined from the UCAC5-calibrated USNO-B1.0, 2MASS, URAT1, and WISE survey positions combined with UCAC5 and GAIA DR1 positions (where available). We find the bright-star and faint-star based proper motions for nearby clusters to be fairly consistent, thereby confirming the validity of the adopted procedure and showing it to introduce no appreciable magnitude-dependent biases.

III. RESULTS

A. PROPER MOTIONS AND THEIR ERRORS

We used the data and technique described above to compute the absolute proper motions of stars in the fields of 115 Milky-Way globular clusters and determine the average absolute proper motions of the clusters. The results are summarized in Table I. Columns 1 and 2 of give the J2000.0 equatorial coordinates of the cluster center, column 3 and 4 give the name and alternative name of the cluster, respectively. Column 5 gives the apparent tidal radius of the cluster in arcmin, columns 6 and 7, the apparent V -band magnitude of the horizontal branch and the apparent V -band distance modulus, respectively. Columns 8 and 9 give the inferred cluster proper-motion component in right ascension and its standard error in mas/yr, respectively, and columns 10 and 11, the proper-motion component in declination and its standard error, respectively. Columns 12 and 13 give the Galactic coordinates the cluster center, and columns 14, 15, 16, and 17 give the average heliocentric radial velocity, heliocentric distance, E_{B-V} color excess, and metallicity $[\text{Fe}/\text{H}]$, respectively. Practically all data except the proper motions (columns 8–11) are adopted from the catalog of Harris [23]. The radial velocities of E3, ESO452-SC11, and Djorg 2 are adopted from the papers [10], [26], and [11], respectively. Figs. 3 and 4 show the distributions of the formal errors of inferred cluster proper motions in right ascension and declination, respectively. The median errors are equal to 0.36 and 0.35 mas/yr for the proper motion in right ascension and declination, respectively. Figs. 5 and 6 show the corresponding transversal-velocity errors, σV_T (RA) and σV_T (DEC), whose median values are equal to 17 and 16 km/s, respectively. Figure 7 shows the dependence of the transversal-velocity error $\langle \sigma V_T \rangle = (\sigma V_T(\text{RA})^2 + \sigma V_T(\text{DEC})^2)^{1/2}$ on

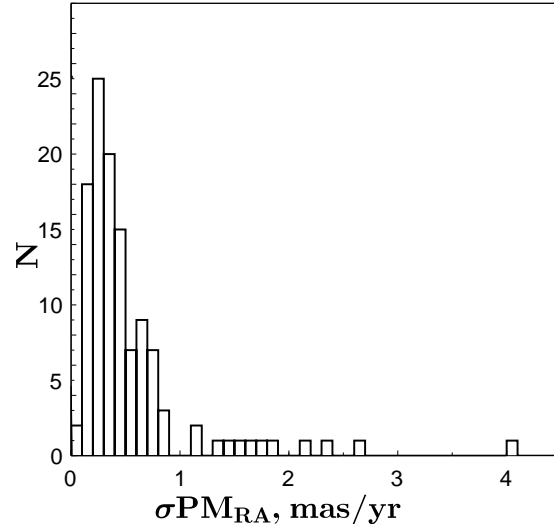


FIG. 3: Distribution of globular-cluster proper-motion errors in right ascension, $\sigma \text{PM}_{\text{RA}}$.

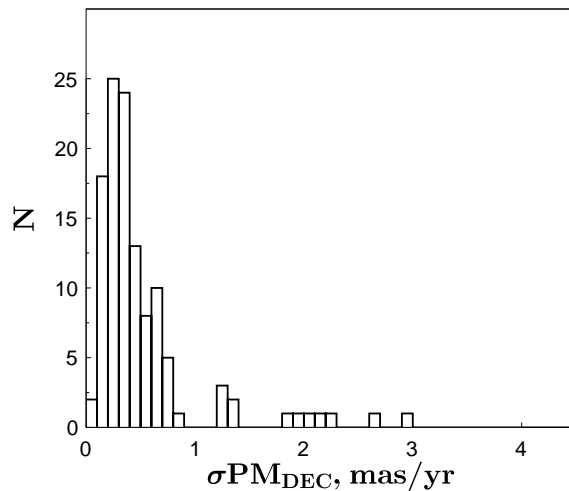


FIG. 4: Distribution of globular-cluster proper-motion errors in declination, $\sigma \text{PM}_{\text{DEC}}$.

heliocentric distance.

IV. GALACTIC POTENTIAL MODEL

In this paper we use a model gravitational potential of the Galaxy, which includes both axisymmetric and non-axisymmetric parts. The axisymmetric part is represented by three components: the Miyamoto and Nagai disk [19], Hernquist spheroid [20], and modified isothermal dark-matter halo. The formulas for the potentials of

TABLE I: Globular cluster data

RA2000	DEC2000	Name	Alternative name	R_{tidal} arcmin	V(HB)	DM	pmra	e_{pmra} mas/yr	pmde	e_{pmde}	l	b	V_r km/s	D_{hel} kpc	E_{B-V}	[Fe/H]
265.1721	-53.6736	NGC 6397		15.811	12.87	12.31	3.34	0.18	-18.00	0.14	338.17	-11.96	18.9	2.2	0.18	-1.95
245.8979	-26.5253	NGC 6121	M 4	32.291	13.45	12.78	-12.64	0.21	-18.26	0.19	350.97	15.97	70.2	2.2	0.36	-1.20
287.7158	-59.9819	NGC 6752		53.759	13.70	13.08	-2.74	0.13	-4.40	0.13	336.50	-25.63	-24.5	3.9	0.04	-1.55
006.0217	-72.0808	NGC 104	47 Tuc	40.570	14.06	13.32	5.41	0.20	-2.79	0.12	305.90	-44.89	-18.7	4.3	0.05	-0.76
279.1008	-23.9033	NGC 6656	M 22	28.993	14.15	13.55	9.36	0.35	-6.62	0.34	9.89	-7.55	-148.9	3.2	0.34	-1.64
294.9975	-30.9622	NGC 6809	M 55	16.285	14.40	13.82	-3.89	0.23	-9.18	0.22	8.80	-23.27	174.8	5.3	0.07	-1.81
298.4421	+18.7783	NGC 6838	M 71	8.899	14.44	13.70	-5.46	0.20	-2.55	0.20	56.74	-4.56	-22.9	3.8	0.25	-0.73
201.6912	-47.4769	NGC 5139	ω Cen	44.835	14.53	13.92	-3.37	0.10	-6.84	0.10	309.10	14.97	232.3	5.1	0.12	-1.62
251.8104	-1.9478	NGC 6218	M 12	15.832	14.60	13.97	0.24	0.84	-6.98	0.74	15.72	26.31	-42.1	4.7	0.19	-1.48
254.2871	-4.0994	NGC 6254	M 10	21.602	14.65	14.03	-4.83	0.37	-6.15	0.29	15.14	23.08	75.8	4.3	0.28	-1.52
154.4033	-46.4111	NGC 3201		29.605	14.80	14.17	9.92	0.19	-2.90	0.35	277.23	8.64	494.0	5.1	0.21	-1.48
140.2471	-77.2825	E 3		10.516	14.80	14.07	-5.56	0.55	2.28	0.55	292.27	-19.02	45.0	4.2	0.30	-0.80
271.8358	-24.9975	NGC 6544		2.133	14.90	14.28	-2.23	0.37	-17.43	0.45	5.84	-2.20	-27.3	2.5	0.74	-1.56
250.4229	+36.4603	NGC 6205	M 13	27.195	14.90	14.28	-3.05	0.48	-1.15	0.48	59.01	40.91	-246.6	7.0	0.02	-1.54
229.6408	+2.0828	NGC 5904	M 5	29.652	15.07	14.41	4.01	0.28	-6.25	0.34	3.86	46.80	52.1	7.3	0.03	-1.29
259.2804	+43.1364	NGC 6341	M 92	14.850	15.10	14.59	-4.16	0.43	-0.56	0.51	68.34	34.86	-121.6	8.1	0.02	-2.29
325.0917	-23.1792	NGC 7099	M 30	18.974	15.10	14.57	0.71	0.40	-7.28	0.40	27.18	-46.83	-184.2	7.9	0.03	-2.12
261.3717	-48.4228	NGC 6352		10.449	15.13	14.39	-2.15	0.21	-4.85	0.21	341.42	-7.17	-120.9	5.6	0.21	-0.70
272.0092	-43.7056	NGC 6541		30.000	15.30	14.72	-1.36	0.34	-6.90	0.36	349.29	-11.18	-156.2	7.4	0.12	-1.83
271.5358	-27.7653	NGC 6540	Djorg 3	9.487	15.30	14.60	-2.89	0.33	-4.88	0.34	3.29	-3.31	-17.7	3.5	0.60	-1.00
186.4392	-72.6592	NGC 4372		34.917	15.30	14.76	-6.45	0.23	2.60	0.30	300.99	-9.88	72.3	4.9	0.42	-2.09
013.1979	-26.5900	NGC 288		12.951	15.30	14.64	3.49	0.69	-5.33	0.44	152.28	-89.38	-46.6	8.1	0.03	-1.24
262.9783	-67.0481	NGC 6362		16.618	15.34	14.65	-5.62	0.31	-5.02	0.26	325.55	-17.57	-13.1	7.5	0.09	-1.06
015.8096	-70.8483	NGC 362		14.806	15.43	14.75	6.47	0.48	-1.55	0.49	301.53	-46.25	223.5	8.3	0.05	-1.16
194.8958	-70.8747	NGC 4833		17.783	15.45	14.87	-7.78	0.14	-1.79	0.18	303.61	-8.01	200.2	5.9	0.33	-1.79
284.8883	-36.6317	NGC 6723		10.547	15.50	14.82	1.20	0.34	-2.80	0.35	0.07	-17.30	-94.5	8.6	0.05	-1.12
280.8029	-32.2919	NGC 6681	M 70	9.487	15.55	14.93	1.14	0.33	-5.70	0.33	2.85	-12.51	218.6	8.7	0.07	-1.51
283.7758	-22.7008	NGC 6717	Pal 9	9.399	15.56	14.90	-4.52	1.16	-5.90	2.08	12.88	-10.90	22.8	7.1	0.21	-1.29
261.9346	-5.0767	NGC 6366		15.221	15.65	14.92	-0.02	0.58	-5.52	0.61	18.41	16.04	-122.3	3.6	0.69	-0.82
205.5467	+28.3756	NGC 5272	M 3	35.397	15.65	15.04	-0.23	0.30	-3.45	0.29	42.21	78.71	-148.6	10.0	0.01	-1.57
189.8667	-26.7428	NGC 4590	M 68	30.120	15.68	15.14	-1.52	0.52	1.17	0.48	299.63	36.05	-95.2	10.1	0.04	-2.06
248.1329	-13.0536	NGC 6171	M 107	17.474	15.70	15.01	-2.49	0.37	-5.83	0.34	3.37	23.01	-33.8	6.3	0.33	-1.04
276.1371	-24.8700	NGC 6626	M 28	11.226	15.70	15.07	-0.24	0.19	-7.97	0.23	7.80	-5.58	17.0	5.7	0.41	-1.45
270.9612	-0.2969	NGC 6535		8.380	15.73	15.15	-6.35	5.07	3.70	5.47	27.18	10.44	-215.1	6.8	0.32	-1.80
322.4929	+12.1669	NGC 7078	M 15	22.136	15.83	15.31	2.04	0.46	-2.15	0.73	65.01	-27.31	-107.5	10.2	0.09	-2.22
278.9404	-32.9903	NGC 6652		4.417	15.85	15.14	-2.39	0.41	-5.14	0.39	1.53	-11.38	-111.7	9.4	0.09	-0.96
277.8467	-32.3481	NGC 6637	M 69	8.346	15.85	15.11	-4.48	0.27	-6.10	0.27	1.72	-10.27	39.9	8.2	0.17	-0.71
244.2604	-22.9750	NGC 6093	M 80	13.369	15.86	15.25	-2.58	0.33	-5.96	0.31	352.67	19.46	9.3	8.7	0.18	-1.62
272.5767	-31.7636	NGC 6558		9.487	15.97	15.34	-1.38	0.12	-5.50	0.20	0.20	-6.03	-143.7	6.4	0.42	-1.44
323.3721	-0.8231	NGC 7089	M 2	21.453	16.05	15.44	1.22	0.33	-2.87	0.40	53.38	-35.78	-5.3	11.4	0.05	-1.62
102.2467	-36.0053	NGC 2298		6.479	16.11	15.54	3.25	0.62	-2.85	0.64	245.63	-16.01	148.9	10.6	0.13	-1.85
078.5262	-40.0472	NGC 1851		13.902	16.15	15.49	1.72	0.48	-0.10	0.44	244.51	-35.04	320.9	12.2	0.02	-1.26
081.0442	-24.5242	NGC 1904	M 79	8.397	16.15	15.53	2.68	0.56	-1.43	0.45	227.23	-29.35	207.5	12.6	0.01	-1.54
289.1479	+30.1847	NGC 6779	M 56	8.674	16.16	15.60	-2.10	2.68	2.33	2.64	62.66	8.34	-135.7	9.9	0.20	-1.94
138.0108	-64.8631	NGC 2808		15.310	16.19	15.55	0.97	0.30	-0.40	0.29	282.19	-11.25	93.6	9.3	0.23	-1.37
283.2679	-8.7061	NGC 6712		7.467	16.25	15.55	3.16	0.29	-5.07	0.28	25.35	-4.32	-107.7	6.7	0.46	-1.01
255.3025	-30.1122	NGC 6266	M 62	9.021	16.25	15.59	-4.50	0.19	-2.46	0.18	353.58	7.32	-65.8	6.7	0.47	-1.29
258.6354	-29.4622	NGC 6304		13.250	16.25	15.49	-2.71	0.30	-1.90	0.28	355.83	5.38	-107.3	6.0	0.52	-0.59
259.7992	-18.5164	NGC 6333	M 9	8.193	16.30	15.71	-2.69	0.27	-4.22	0.26	5.54	10.70	229.1	8.3	0.36	-1.72
277.9762	-23.4764	NGC 6642		9.772	16.30	15.65	0.33	0.21	-4.32	0.18	9.81	-6.44	-57.2	7.6	0.40	-1.35
229.3521	-21.0103	NGC 5897		12.085	16.35	15.77	-6.36	0.43	-3.97	0.46	342.95	30.29	101.5	12.7	0.08	-1.80
255.6571	-26.2681	NGC 6273	M 19	14.570	16.40	15.80	-4.27	0.21	1.04	0.21	356.87	9.38	135.0	8.5	0.37	-1.68
269.7583	-44.2650	NGC 6496		5.262	16.47	15.72	-2.62	0.37	-9.14	0.41	348.02	-10.01	-112.7	11.6	0.13	-0.64
257.5433	-26.5817	NGC 6293		15.811	16.50	15.94	0.65	0.16	-3.97	0.16	357.62	7.83	-98.9	8.8	0.39	-1.92
236.5146	-37.7861	NGC 5986		10.455	16.50	15.90	-3.61	0.32	-4.66	0.30	337.02	13.27	88.9	10.3	0.27	-1.67
277.7342	-25.4964	NGC 6638		6.531	16.50	15.80	-2.64	0.29	-3.18	0.29	7.90	-7.15	18.1	8.2	0.40	-0.99
206.6104	-51.3733	NGC 5286		8.364	16.50	15.90	-0.25	0.35	0.48	0.33	311.61	10.57	58.3	10.7	0.24	-1.67
274.6571	-52.2150	NGC 6584		9.351	16.53	15.90	0.70	0.34	-6.58	0.35	342.14	-16.41	222.9	13.0	0.11	-1.49
246.4525	-72.2017	NGC 6101		7.256	16.60	16.02	2.25	0.42	0.78	0.46	317.75	-15.82	361.4	15.1	0.04	-1.82
232.0021	-50.6728	NGC 5927		16.721	16.60	15.81	-5.02	0.15	-3.00	0.15	326.60	4.86	-115.7	7.4	0.47	-0.37
246.8087	-26.0247	NGC 6144		33.352	16.60	16.01	-4.58	0.93	-11.68	2.35	351.93	15.70	188.9	10.1	0.32	-1.73
272.3150	-25.9078	NGC 6553		8.135	16.60	15.79	-2.35	0.29	-2.35	0.27	5.25	-3.02	-6.5	4.7	0.78	-0.25
211.3637	+28.5344	NGC 5466		52.754	16.62	16.10	-5.08	0.51	-2.10	0.55	42.15	73.59	107.7	16.6	0.00	-2.22
199.1125	+17.6981	NGC 5053		14.866	16.65	16.14	-1.50	2.00	-2.10	1.85	335.69	78.94	44.0	16.2	0.03	-2.29
249.8562	-28.3978	1636-283	ESO452-SC11	7.697	16.66	15.96	-7.30	1.60	-3.50	1.40	351.91	12.10	17.5	7.6	0.50	-1.15

TABLE I: End

RA2000	DEC2000	Name	Alternative name	R_{tidal} arcmin	V(HB)	DM	pmra	e_{pmra} mas/yr	pmde	e_{pmde}	l	b	V_r km/s	Rh kpc	E_{B-V}	[Fe/H]
253.3558	-22.1772	NGC 6235		7.262	16.70	16.06	-3.52	1.26	-5.89	1.29	358.92	13.52	87.3	9.7	0.36	-1.40
048.0637	-55.2169	NGC 1261		9.171	16.70	16.05	1.41	0.76	-2.67	0.71	270.54	-52.13	68.2	16.0	0.01	-1.35
308.5483	+7.4042	NGC 6934		15.811	16.90	16.28	-1.92	0.32	-5.25	0.34	52.10	-18.89	-411.4	15.2	0.12	-1.54
198.2304	+18.1692	NGC 5024	M 53	8.471	16.90	16.36	-0.66	1.07	-0.30	0.80	332.96	79.76	-79.1	18.4	0.01	-2.07
313.3662	-12.5369	NGC 6981	M 72	22.295	16.90	16.28	-0.85	0.49	-3.02	0.44	35.16	-32.68	-345.1	16.8	0.05	-1.54
260.2925	-19.5872	NGC 6342		10.351	16.90	16.15	-2.24	2.57	-8.23	2.54	4.90	9.73	80.9	9.1	0.44	-0.65
256.2892	-22.7081	NGC 6287		6.310	17.00	16.46	-4.62	0.54	-1.65	0.63	0.13	11.02	-208.0	8.4	0.59	-2.05
182.5258	+18.5419	NGC 4147		17.549	17.01	16.43	-0.63	2.15	-0.62	2.12	252.85	77.19	183.2	18.8	0.02	-1.83
273.4121	-31.8264	NGC 6569		17.419	17.10	16.38	-1.78	0.28	-7.45	0.24	0.48	-6.68	-28.1	8.5	0.56	-0.86
267.5537	-37.0511	NGC 6441		6.890	17.10	16.33	-4.07	0.30	-4.40	0.34	353.53	-5.01	18.3	9.7	0.45	-0.53
326.6617	-21.2508	Pal 12		33.043	17.13	16.42	-0.77	0.73	-2.36	0.69	30.51	-47.68	27.8	18.7	0.02	-0.93
264.4004	-3.2458	NGC 6402	M 14	15.811	17.20	16.56	-3.45	1.70	-6.57	1.50	21.32	14.81	-66.1	8.7	0.60	-1.39
264.0708	-44.7350	NGC 6388		13.554	17.25	16.49	-1.00	0.16	-2.52	0.16	345.56	-6.74	81.2	11.5	0.38	-0.60
280.3746	-19.8258	Pal 8		22.136	17.27	16.49	-3.13	0.27	-5.89	0.29	14.10	-6.80	-43.0	12.4	0.33	-0.48
256.1200	-24.7647	NGC 6284		9.796	17.30	16.65	-3.00	0.28	-0.30	0.27	358.35	9.94	29.7	14.3	0.28	-1.32
296.3100	-8.0072	Pal 11		7.586	17.35	16.56	-0.94	0.55	-2.97	0.53	31.81	-15.58	-68.0	12.6	0.34	-0.39
301.5200	-21.9214	NGC 6864	M 75	7.975	17.47	16.82	-0.51	0.87	-2.17	0.87	20.30	-25.75	-189.3	18.4	0.16	-1.32
287.8004	+1.0306	NGC 6760		15.937	17.50	16.73	0.87	0.31	-2.51	0.31	36.11	-3.92	-27.5	7.3	0.78	-0.52
260.8958	-17.8131	NGC 6356		12.838	17.50	16.73	-4.40	0.17	-5.12	0.19	6.72	10.22	27.0	14.6	0.29	-0.50
225.0771	-82.2136	IC 4499		12.244	17.65	17.04	0.12	0.79	-3.20	0.73	307.35	-20.47	31.5	18.4	0.23	-1.60
267.7158	-34.5986	NGC 6453		8.360	17.70	17.08	-0.96	0.24	-4.00	0.25	355.72	-3.87	-83.7	10.9	0.61	-1.53
264.6537	-23.9089	NGC 6401		22.136	17.70	17.02	-4.18	0.26	-2.32	0.28	3.45	3.98	-65.0	7.5	0.85	-1.12
217.4054	-5.9764	NGC 5634		7.334	17.75	17.17	-5.25	2.20	-1.87	2.23	342.21	49.26	-45.1	25.3	0.05	-1.82
289.4321	-34.6575	Terzan 7		6.032	17.76	17.00	-1.74	0.73	-2.70	0.65	3.39	-20.07	166.0	23.0	0.06	-0.58
259.1558	-28.1400	NGC 6316		5.012	17.78	17.01	-4.52	0.48	-3.70	0.47	357.18	5.76	71.5	11.5	0.55	-0.55
189.6675	-51.1503	Rup 106		25.298	17.80	17.22	-5.31	0.53	-4.57	0.55	300.89	11.67	-44.0	20.6	0.21	-1.80
233.8687	-50.6594	NGC 5946		2.194	17.80	17.16	-5.61	0.41	-1.38	0.43	327.58	4.19	119.5	12.3	0.55	-1.38
246.9183	-38.8489	NGC 6139		1.328	18.00	17.40	-8.04	0.29	-2.93	0.29	342.37	6.94	6.7	10.5	0.74	-1.65
251.7454	+47.5278	NGC 6229		8.833	18.00	17.37	-1.48	2.50	1.45	1.76	73.64	40.31	-154.2	29.3	0.01	-1.44
295.4375	-34.0003	Terzan 8		13.031	18.03	17.46	-1.31	0.67	-3.25	0.67	5.76	-24.56	130.0	25.4	0.14	-1.87
283.7637	-30.4783	NGC 6715	M 54	6.325	18.17	17.56	-2.82	0.78	-2.47	0.34	5.61	-14.09	141.9	26.2	0.15	-1.59
254.8858	-37.1214	NGC 6256		9.487	18.20	17.45	-2.42	0.52	-0.97	0.48	347.79	3.31	-99.5	9.3	0.84	-0.70
259.4967	-23.7658	NGC 6325		21.498	18.30	17.63	-8.26	1.24	-6.63	1.06	0.97	8.00	3.1	9.4	0.89	-1.17
271.2075	-7.5858	NGC 6539		21.058	18.33	17.58	-7.26	4.10	-6.96	2.96	20.80	6.78	-45.6	7.9	1.00	-0.66
272.6842	-7.2075	IC 1276	Pal 7	14.092	18.40	17.70	-6.46	0.54	-6.57	0.51	21.83	5.67	155.0	9.3	0.92	-0.56
225.9937	-33.0678	NGC 5824		4.151	18.45	17.88	-1.98	1.80	-1.01	2.21	332.55	22.07	-38.4	31.3	0.13	-1.85
219.9021	-26.5383	NGC 5694		9.487	18.50	17.93	-1.35	1.52	-1.43	1.29	331.06	30.36	-145.8	33.9	0.09	-1.86
267.2192	-20.3594	NGC 6440		5.914	18.70	17.90	-3.96	1.28	-4.08	0.97	7.73	3.80	-78.7	8.0	1.09	-0.34
247.1671	-35.3536	Terzan 3		6.313	18.80	18.10	-5.71	1.28	-2.66	0.77	345.08	9.19	-136.3	26.4	0.32	-0.73
264.0437	-38.5533	Ton 2	Pismis 26	3.964	19.10	18.33	-1.64	0.89	-4.36	1.27	350.80	-3.42	-184.4	7.9	1.24	-0.50
136.9908	-37.2214	Pyxis		10.436	19.25	18.58	-2.00	0.90	2.80	1.30	261.32	7.00	34.3	38.5	0.21	-1.20
270.4546	-27.8258	Djorg 2	E456-SC38	5.206	19.50	18.80	-3.26	0.29	-3.47	0.28	2.76	-2.51	-150.0	13.8	1.00	-0.50
286.3137	+1.9008	NGC 6749		8.309	19.70	19.09	-3.80	0.39	-4.60	0.35	36.20	-2.20	-61.7	7.7	1.50	-1.60
265.9258	-26.2225	Pal 6		3.080	19.70	18.87	-7.72	0.46	-6.96	0.47	2.09	1.78	201.0	6.7	1.53	-0.10
261.7854	-7.0931	IC 1257		12.649	19.80	19.20	-3.54	0.64	-1.69	0.63	16.53	15.14	140.2	24.5	0.73	-1.70
263.9492	-30.4697	Terzan 1	HP 2	4.817	19.95	19.15	1.44	0.75	-3.47	0.41	357.57	1.00	35.0	6.5	1.64	-0.35
261.8892	-30.8022	Terzan 2	HP 3	3.147	20.10	19.29	-3.38	0.28	-3.63	0.29	356.32	2.30	109.0	9.5	1.42	-0.25
266.8679	-33.0656	Djorg 1		2.038	20.80	20.10	-7.97	0.63	-3.73	0.60	356.67	-2.48	-362.4	9.2	1.70	-0.40
071.5246	+31.3808	Pal 2		9.892	21.65	20.99	7.19	0.62	0.27	0.63	170.53	-9.07	-133.0	26.9	1.24	-1.30
268.6133	-24.1453	UKS 1		11.972	24.14	23.47	-2.78	0.51	-0.55	0.54	5.12	0.76	57.0	7.5	2.93	-1.20

these three components have the following form:

$$\phi_{spher} = -\frac{GM_{spher}}{\sqrt{R^2 + z^2 + c}} \quad (2)$$

$$\phi_{disk} = -\frac{GM_{disk}}{\sqrt{R^2 + (a + \sqrt{z^2 + b^2})^2}} \quad (1)$$

$$\phi_{halo} = V_{halo}^2 \ln(R^2 + z^2 + d^2) \quad (3)$$

Here we use the following parameter values: $M_{disk} = 10^{11} M_{sun}$, $a = 5$, $b = 0.26$, $M_{spher} = 3.4 \times 10^{10} M_{sun}$, $c =$

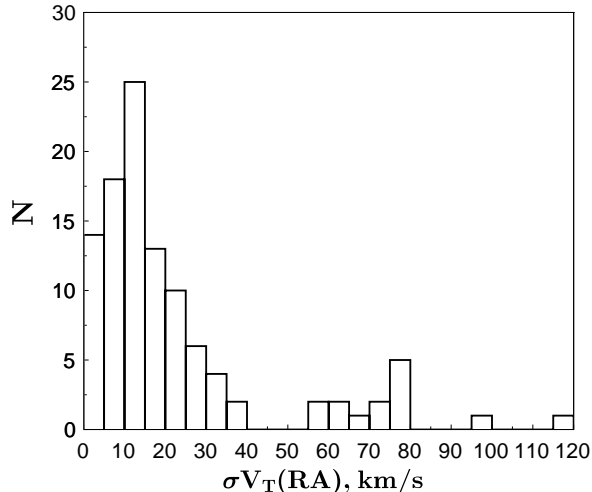


FIG. 5: Distribution of transversal-velocity errors σ_T (RA) in right ascension for 106 globular clusters with $\sigma_P M_{RA} \leq 1$ mas/yr and $\sigma_P M_{DEC} \leq 1$ mas/yr.

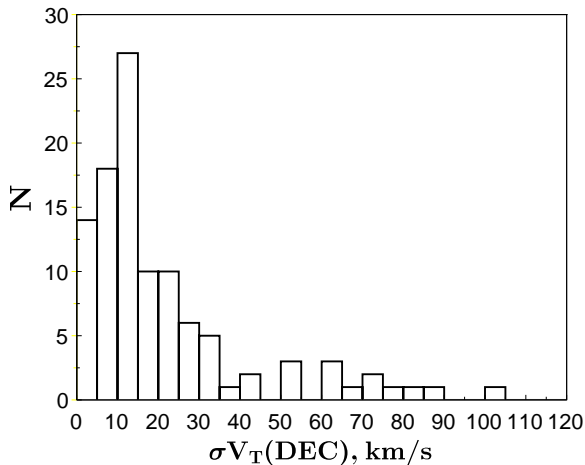


FIG. 6: Distribution of transversal-velocity errors σ_T (DEC) in declination for 106 globular clusters with $\sigma_P M_{RA} \leq 1$ mas/yr and $\sigma_P M_{DEC} \leq 1$ mas/yr.

0.7, $V_{halo} = 1.15$, $d = 12$ (all distances are in kpc). We choose these constants so as to ensure that the resulting rotation curve in the Galactic disk would fit the rotation curve based on recent data about the kinematics of Galactic masers [21], implying a circular velocity rotation of about 237 km/s at the solar circle (we adopt $R_0 = 8.3$ kpc throughout this paper).

The non-axisymmetric part of the gravitational potential is represented by the Galactic bar, which we modeled by a Ferrer's bar with index $n = 2$ [22]. In this model the bar has the shape of an ellipsoid of rotation with the semimajor and semiminor axes equal to $a_{bar} = 4$ kpc

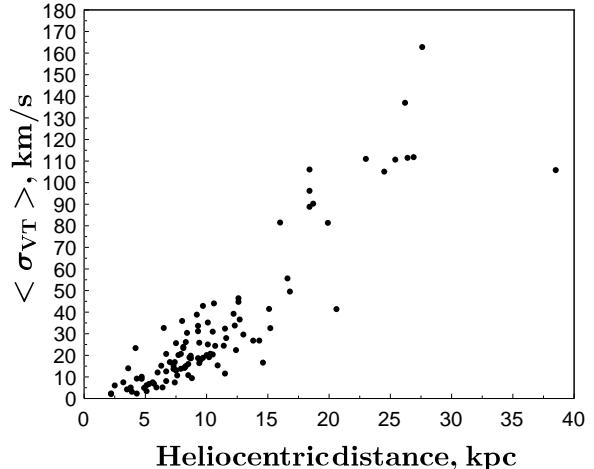


FIG. 7: Dependence of the transversal-velocity error $\langle \sigma_{VT} \rangle = (\sigma_{VT}(RA)^2 + \sigma_{VT}(DEC)^2)^{1/2}$ on heliocentric distance for 106 globular clusters with $\sigma_P M_{RA} \leq 1$ mas/yr and $\sigma_P M_{DEC} \leq 1$ mas/yr.

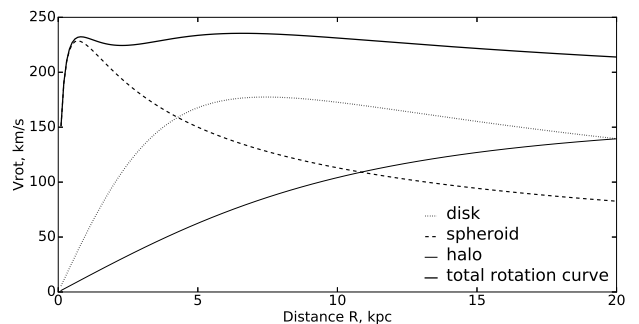


FIG. 8: Decomposition of the rotation curve based on the axisymmetric part of the Galactic gravitational potential

and $c_{bar} = 1$ kpc, respectively, and the axis of rotation located in the symmetry plane of the Galaxy. The density distribution in the adopted bar model has the form:

$$\rho = \begin{cases} \rho_0(1 - m^2)^2 & m < 1 \\ 0 & m \geq 1 \end{cases} \quad (4)$$

where $m^2 = x^2/a_{bar}^2 + (y^2 + z^2)/c_{bar}^2$. The formula for the gravitational potential in the Cartesian coordinate system associated with the bar (the x -axis directed along the semimajor axis of the bar, the z -axis points toward the North Galactic Pole, and the y -axis directed along the semiminor axis of the bar so as to make the right-

handed coordinate system) has the following form:

$$\begin{aligned} \phi_{bar} = & -\frac{105GM_{bar}}{32\varepsilon} \left[\frac{1}{3}w_{10} - \left((y^2 + z^2)w_{20} + \right. \right. \\ & + x^2w_{11} \left. \right) + \left((y^2 + z^2)^2 w_{30} + 2(y^2 + z^2)x^2w_{21} + \right. \\ & + x^4w_{12} \left. \right) - \frac{1}{3} \left((y^2 + z^2)^3 w_{40} + 3(y^2 + z^2)^2 x^2w_{31} + \right. \\ & \left. \left. + 3(y^2 + z^2)x^4w_{22} + x^6w_{13} \right) \right] \quad (5) \end{aligned}$$

where $\varepsilon^2 = a_{bar}^2 - c_{bar}^2$. The coordinates x, y, z in equation 5 are nondimensionalized by dividing them by parameter ε . The integrated coefficients w_{ij} are defined as:

$$w_{ij}(\psi) = 2 \int_0^\psi \tan^{2i-1} \theta \sin^{2j-1} \theta d\theta \quad (6)$$

where $\psi(x, y, z)$ is the function of coordinates equal to the solution of the equation

$$\begin{aligned} (y^2 + z^2) \tan^2 \psi + x^2 \sin^2 \psi &= \varepsilon^2 & m > 1 \\ \cos \psi &= c_{bar}/a_{bar} & m \leq 1 \end{aligned} \quad (7)$$

Throughout this study we assumed that at the present time the orientation angle of the bar with respect to the Galactic center–Sun direction is equal to 45° (the first quadrant). We assumed the angular velocity and mass of the bar to be 50 km/s/kpc and 10% of the Galactic disk mass ($M_{bar} = 10^{10} M_{sun}$).

V. ORBITS

We computed the orbits of 115 Milky-Way globular clusters in terms of two models of the gravitational potential of the Galaxy: a purely axisymmetric model (disk+spheroid+halo) and a model, which, in addition to the above three components includes a rotating bar. Five of 115 clusters – Terzan 3, NGC 5634, Rup 106, Pyxis, and Pal 2 – have escaping trajectories, which are most likely due to large errors of the inferred proper motions of these clusters resulting in the total velocities greater than the escape velocities at the corresponding locations (all these clusters are quite far away from the Sun at heliocentric distances ranging from 20.6 to 38.5 kpc, which explain the large errors of their proper motions and transversal velocities). We computed the orbits of all clusters orbits for 2-Gyr forward, except for IC 1257, NGC 6101, NGC 6229, and NGC 6715. The latter four clusters are too distant to make more than one revolution within 2 Gyr and we integrated their orbits for 5 Gyr forward. The parameters of the resulting globular-cluster orbits are listed in Tables II (for the model potential without the bar) and III (for the model potential with a bar). The full versions of Tables II and III and images of the

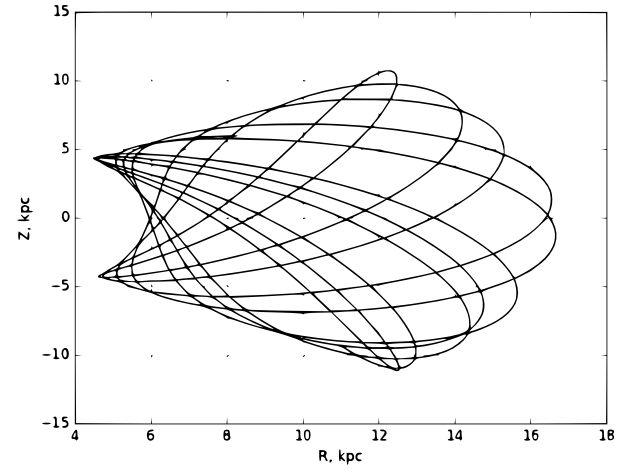
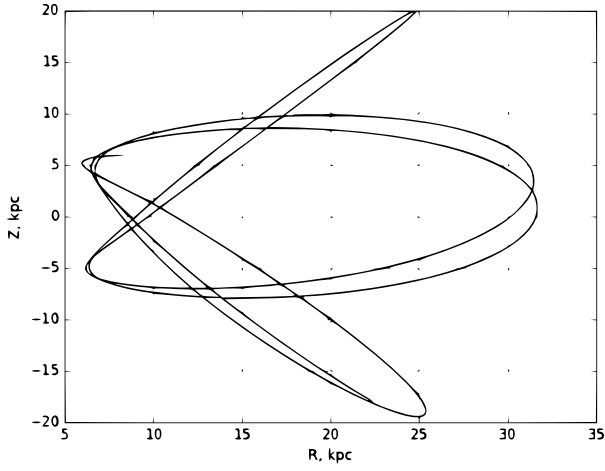
orbits of all clusters are available in electronic form at www.sai.msu.ru/groups/cluster/cl/orbits_gcl/ Table II gives the following quantities: cluster name; $(R_{min})_{min}$ and $\langle R_{min} \rangle$ (the minimum and average pericentric distance, respectively); $(R_{max})_{max}$ and $\langle R_{max} \rangle$ (the maximum and average apocentric distance, respectively); $(|z|_{max})_{max}$ and $\langle |z|_{max} \rangle$ (the maximum and average distance from the symmetry plane of the Galaxy, respectively); $\langle e \rangle$, the estimated average eccentricity of the cluster orbit; E , the total mechanical energy per unit mass of the cluster in 100km/s^2 , and h , the projection of the specific angular momentum of the cluster onto the symmetry axis of the Galaxy (in $100 \text{ kpc} \cdot \text{km/s}$). All distances are in kpc. In the case of the axisymmetric model potential E and h are conserved. Table III differs from Table III in that it gives the minimum, maximum, and average values of E and h (E_{min} , E_{max} , E_{avg} , h_{min} , h_{max} , and h_{avg}) because the total mechanical energy and projection of the orbital momentum onto the Galactic symmetry axis are not conserved in the case of the barred potential (the bar brings explicit dependence on time and angle into the Hamiltonian of the cluster). When computing the total mechanical energy of the cluster we set the gravitational potential equal to zero at the Galactocentric distance of 300 kpc (adopted boundary of the Galaxy). Figs. 9 and 10 show the meridional cross sections and galactic-plane projections of three globular clusters (the metal-poor clusters NGC 4590 and NGC 6266 and the metal-rich cluster NGC 6316) computed with axisymmetric potential (the figures on the left) and with the barred potential (the figures on the right). Interestingly, the correlation between the metallicity and average eccentricity, which shows up conspicuously in for orbits computed with axisymmetric potential with the most metal-poor clusters have almost exclusively high eccentricities (Fig. 11) disappears if the orbits are computed in the barred potential (Fig. 12).

Unlike the conclusions reached by the authors of the so far most extensive observational study of the orbits of a total of 54 Galactic globular clusters [1, 2], we find that the bar has appreciable effect on the orbits of all clusters: it destroys the orbital boxes and randomizes (chaotizes) the orbits. The effect of the bar on distant orbits is weaker (central parts of the orbits mostly get entangled), which is to be expected given the 10% contribution of the bar to the effective mass. Orbits of some of the thick-disk clusters are literally "stretched out" by the bar and become, on the average, closer to the Galactic center. Typical examples include such clusters as E3, NGC 104, and NGC 5927 whose orbits we show in Figs. 13 and 14. We defer a more detailed analysis of the cluster orbits to our forthcoming paper.

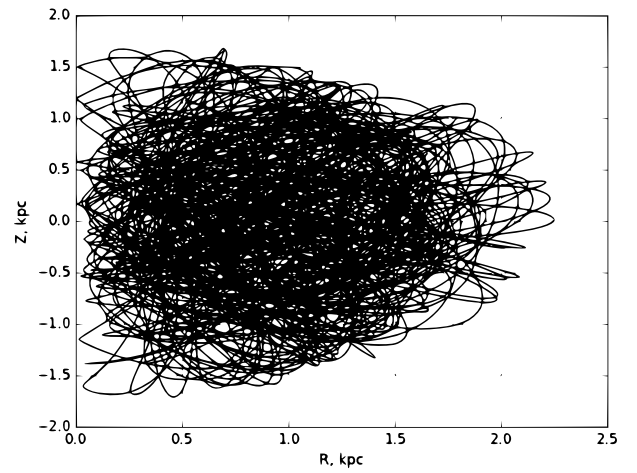
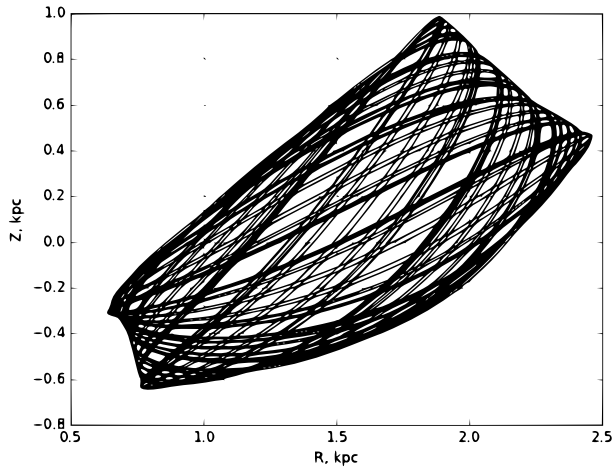
VI. CONCLUSIONS

We determined accurate absolute proper motions (with a typical accuracy of $\sim 0.4 \text{ mas/yr}$, which translates into

NGC 4590 ([Fe/H]=-2.06)



NGC 6266 ([Fe/H]=-1.29)



NGC 6316 ([Fe/H]=-0.55)

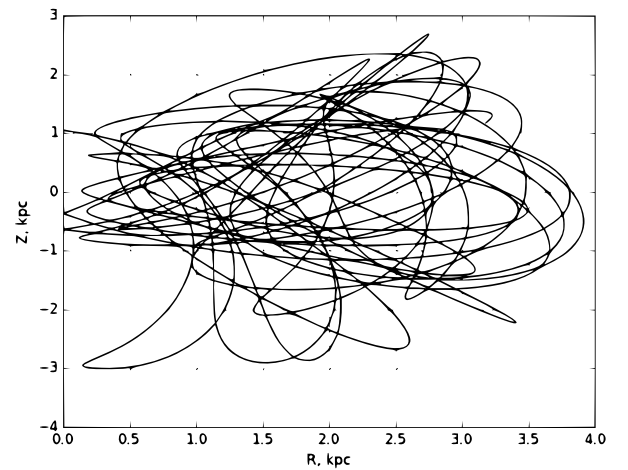
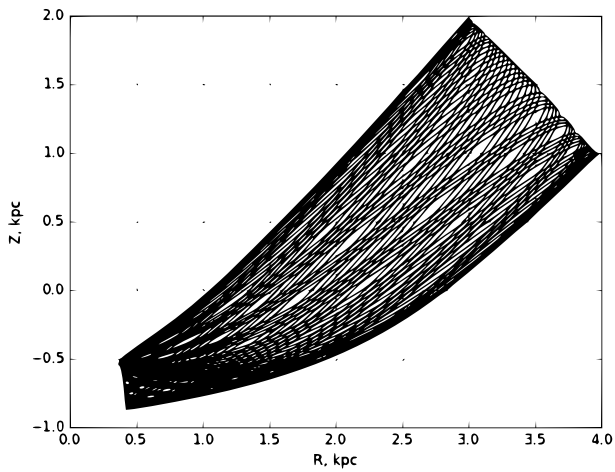
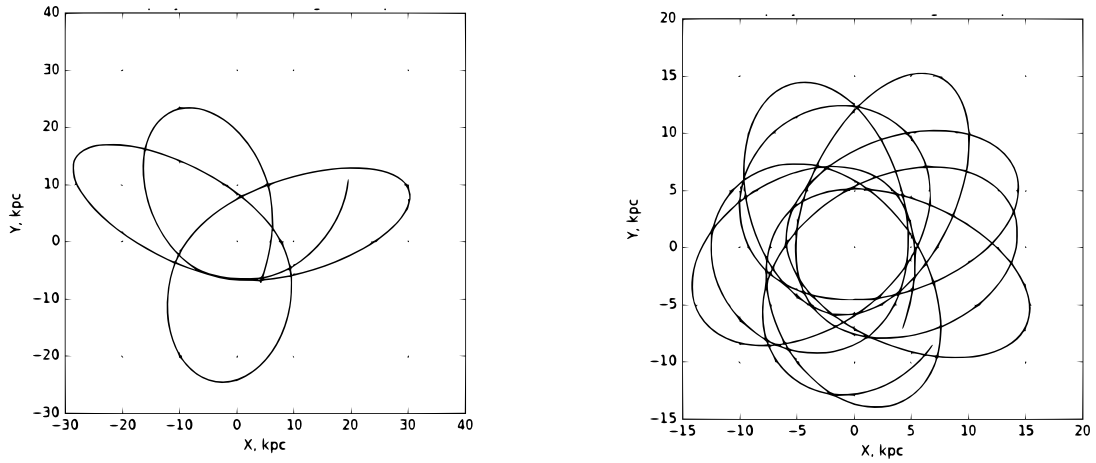
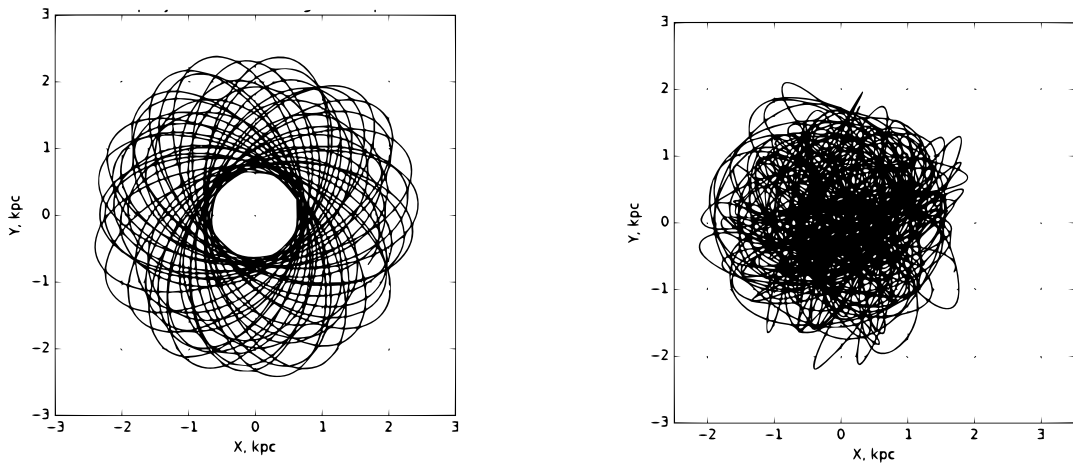


FIG. 9: Meridional cross sections of the orbits of the globular clusters NGC 4590, NGC 6266, and NGC 6316) computed with axisymmetric potential (on the left) and with the barred potential (on the right). Chaotization caused by the bar is especially evident in the case of NGC 6266 and NGC 6316.

NGC 4590 ($[Fe/H]=-2.06$)



NGC 6266 ($[Fe/H]=-1.29$)



NGC 6316 ($[Fe/H]=-0.55$)

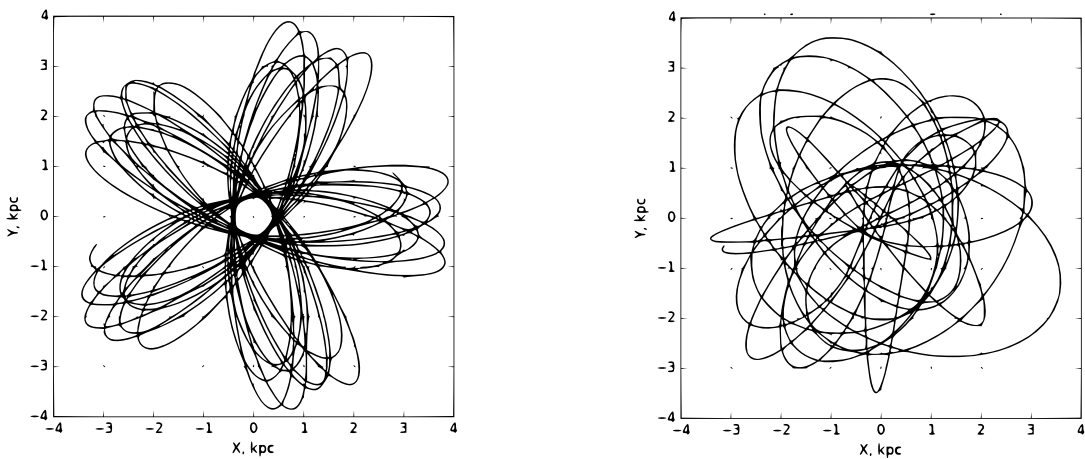


FIG. 10: Galactic-plane projections of the orbits of the globular clusters NGC 4590, NGC 6266, and NGC 6316) computed with axisymmetric potential (on the left) and with the barred potential (on the right). Like in the case of meridional cross sections, chaoticization caused by the bar is especially evident in the case of NGC 6266 and NGC 6316.

TABLE II: Results of the analysis of cluster orbits in the potential model without the bar

Name	$(R_{min})_{min}$	$\langle R_{min} \rangle$	$(R_{max})_{max}$	$\langle R_{max} \rangle$	$(z _{max})_{max}$	$\langle z _{max} \rangle$	$\langle e \rangle$	E	h
1636-283	0.04	0.05	3.10	2.43	2.11	0.88	0.96	-18.89	0.22
IC 1257	7.15	8.57	86.05	67.22	70.86	44.74	0.77	-3.56	26.19
IC 4499	4.28	7.62	61.37	35.20	58.84	33.44	0.64	-4.53	13.18

TABLE III: Results of the analysis of cluster orbits in the potential model with a bar

Name	$(R_{min})_{min}$	$\langle R_{min} \rangle$	$(R_{max})_{max}$	$\langle R_{max} \rangle$	$(z _{max})_{max}$	$\langle z _{max} \rangle$	$\langle e \rangle$	E_{min}	E_{max}	E_{avg}	h_{min}	h_{max}	h_{avg}
NGC 1261	0.03	0.54	22.65	15.83	9.81	3.26	0.93	-15.83	-9.34	-12.77	-1.58	11.11	4.40
NGC 1851	0.07	0.23	21.68	15.98	23.19	8.55	0.97	-11.72	-6.82	-10.11	-4.40	5.19	-1.25
NGC 1904	0.10	0.28	31.66	16.15	19.93	6.90	0.97	-14.36	-8.19	-11.34	-6.62	5.44	-0.71

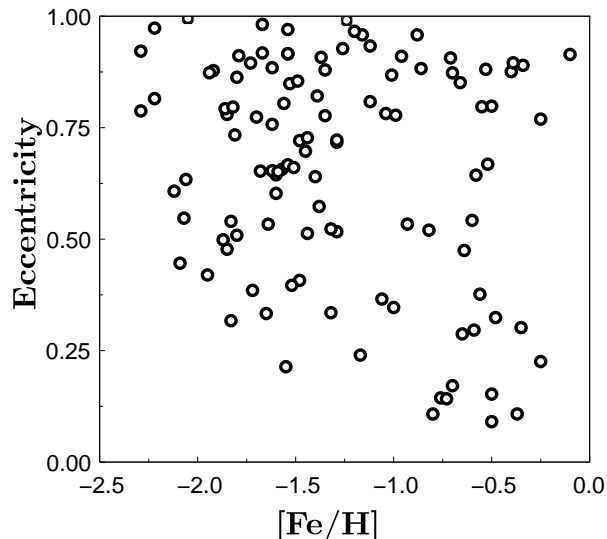


FIG. 11: Metallicity vs. average eccentricity plot for orbits computed in terms of axisymmetric potential model.

a ~ 17 km/s transversal-velocity error) and computed Galactic orbits for the currently largest sample of Galactic globular clusters (115 objects), which represents a two-fold increase compared to the most extensive previous studies. We computed the cluster orbits in terms of both an axisymmetric potential model and a model with a rotating bar. Unlike what was found by the authors of earlier studies, we conclude that the bar has appreciable effect on the orbits of practically all clusters in that it randomizes the orbits and especially their portions in the vicinity of the Galactic center, and stretches out the orbits of some of the thick-disk clusters.

ACKNOWLEDGEMENTS

This work has made use of data from the European Space Agency (ESA) mission *Gaia* (<https://www.cosmos.esa.int/gaia>),

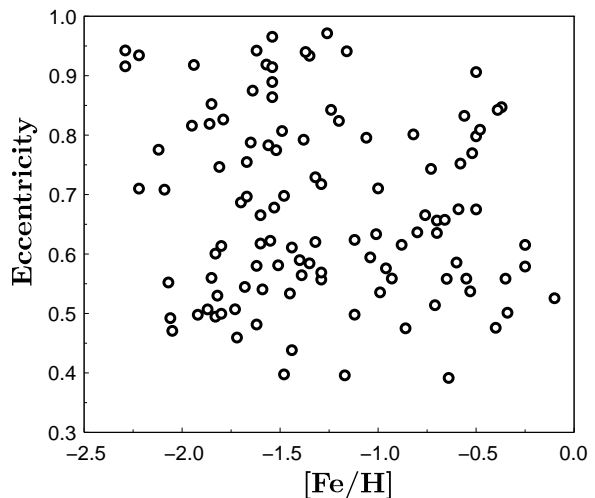


FIG. 12: Metallicity vs. average eccentricity plot for orbits computed in terms of barred potential model.

processed by the *Gaia* Data Processing and Analysis Consortium (DPAC, <https://www.cosmos.esa.int/web/gaia/dpac/consortium>). Funding for the DPAC has been provided by national institutions, in particular the institutions participating in the *Gaia* Multilateral Agreement. This publication makes use of data products from the Two Micron All Sky Survey, which is a joint project of the University of Massachusetts and the Infrared Processing and Analysis Center/California Institute of Technology, funded by the National Aeronautics and Space Administration and the National Science Foundation, and of the data products from the Wide-field Infrared Survey Explorer, which is a joint project of the University of California, Los Angeles, and the Jet Propulsion Laboratory/California Institute of Technology, and NEOWISE, which is a project of the Jet Propulsion Laboratory/California Institute of Technology. WISE and NEOWISE are funded by the National Aeronautics and Space Administration.. This work was supported by the Russian Foundation for

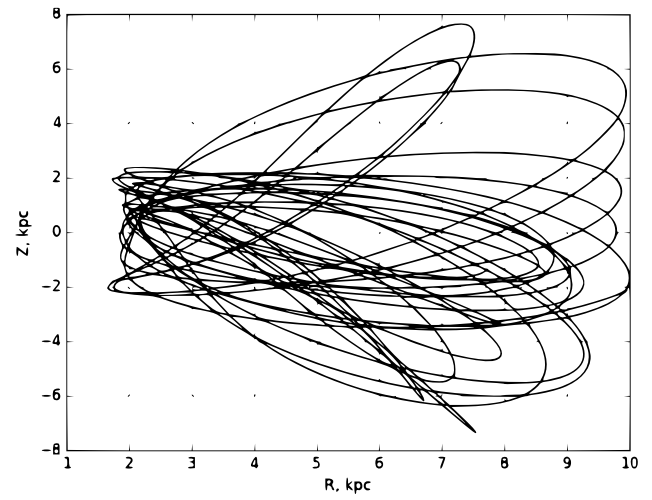
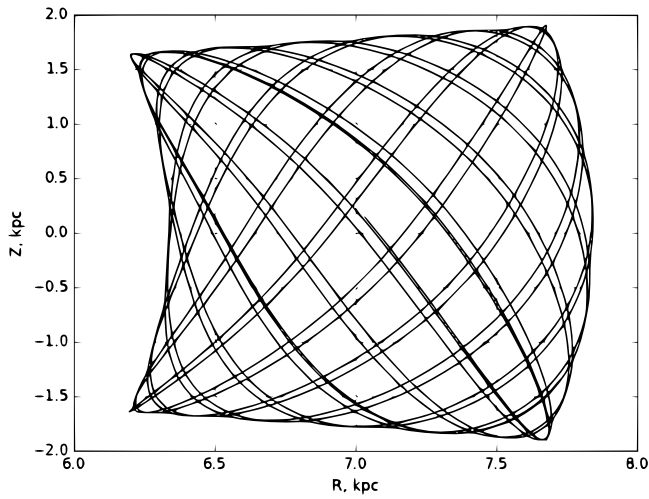
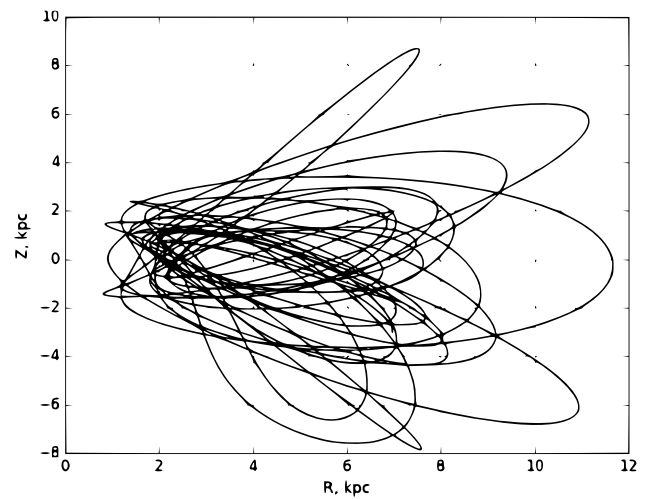
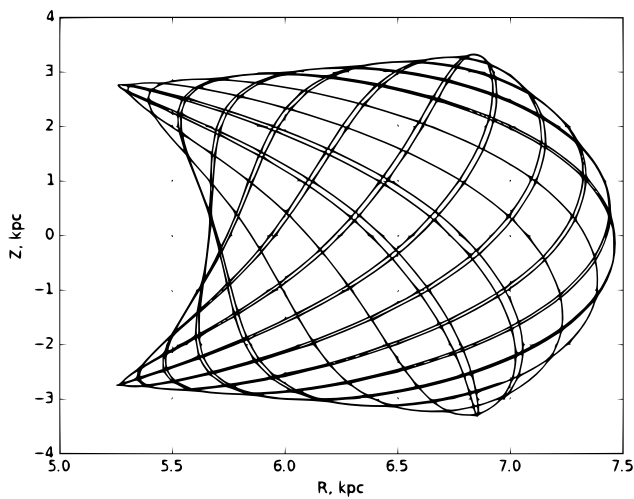
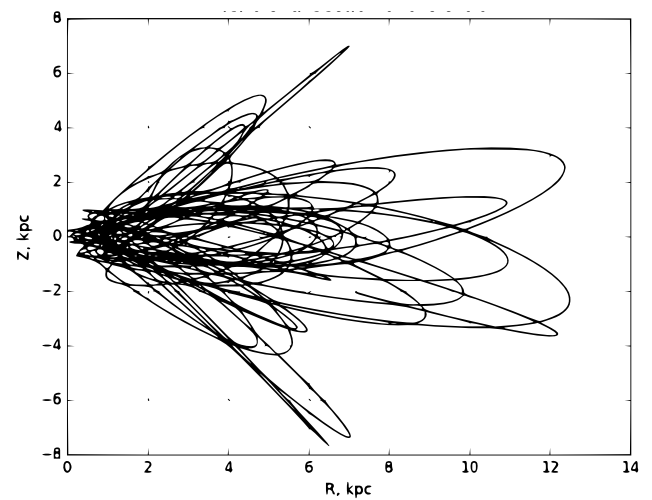
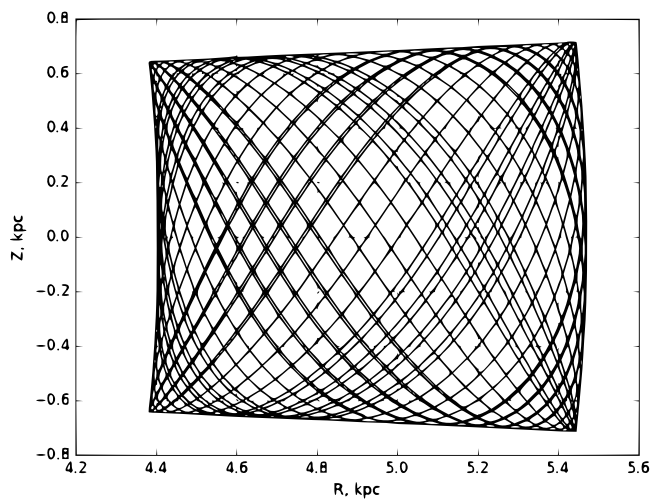
E3 ([Fe/H]=-0.80)**NGC 104 ([Fe/H]=-0.76)****NGC 5927 ([Fe/H]=-0.37)**

FIG. 19. Multi-dimensional phase space plots of the orbits of the globular clusters E3, NGC 104, and NGC 5927. The left column shows the phase space plots in the R-Z plane, and the right column shows the phase space plots in the R-Z plane.

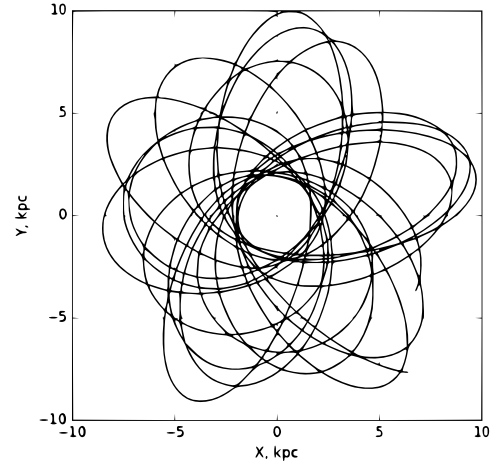
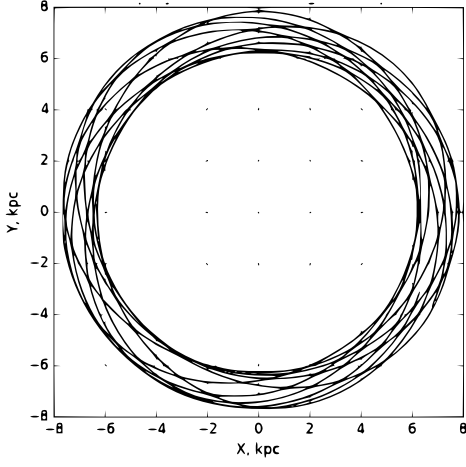
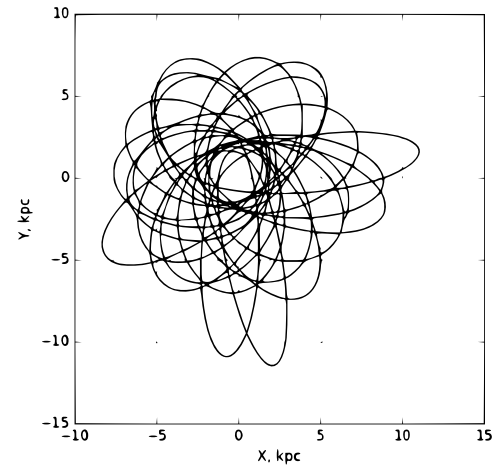
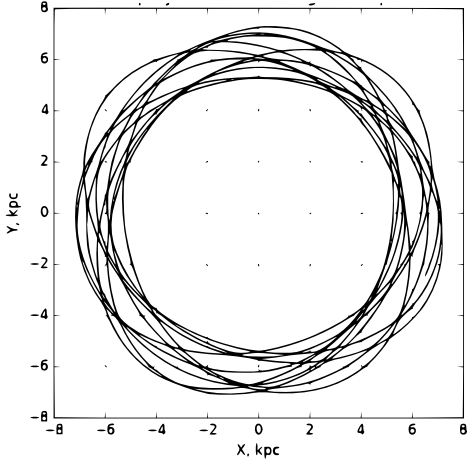
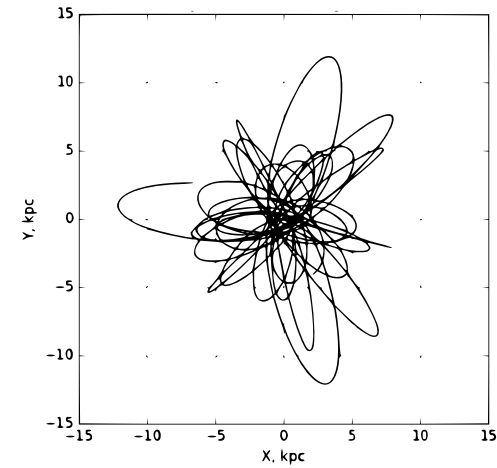
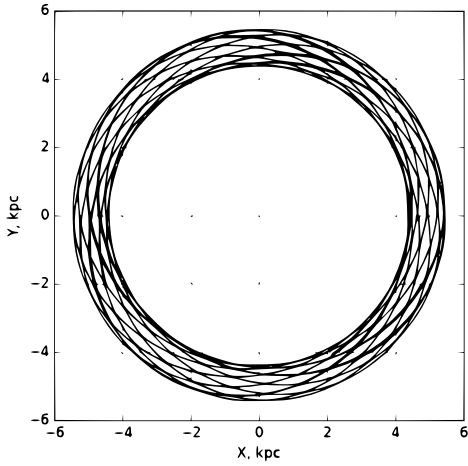
E3 ([Fe/H]=-0.80)**NGC 104 ([Fe/H]=-0.76)****NGC 5927 ([Fe/H]=-0.37)**

FIG. 14: Galactic-plane projections of the orbits of the globular clusters E3, NGC 104, and NGC 5927) computed with axisymmetric potential (on the left) and with the barred potential (on the right).

Basic Research (grant no. 18-02-00890).

-
- [1] Allen, Ch., Moreno, E., Picardo, B., ApJ **652**, 1150 (2006)
- [2] Allen, Ch., Moreno, E., Picardo, B., ApJ **674**, 237 (2008)
- [3] Bovy, J. et al., ApJ **759**, 131 (2012)
- [4] D.I. Casetti-Dinescu, T. M. Girard, L. Jilkova, et al. Astron. J. **146**, 33 (2013)
- [5] D.I. Casetti-Dinescu, T. M. Girard, V. I. Korchagin, et al. Astron. J. **140**, 1282 (2010)
- [6] D.I. Casetti-Dinescu, T. M. Girard, D. Herrera, et al. Astron. J. **124**, 195(2007)
- [7] M.-R.L. Cioni, K. Bekki, L. Girardi et al. Astron. and Astrophys. **586**, 77 (2016)
- [8] A. K. Dambis, Astron. Astrophys. Trans. **25**, 185 (2006)
- [9] A.K. Dambis, Monthly Notices Royal Astron. Soc. **396**, 553 (2009)
- [10] R. de la Fuente Marcos, C. de la Fuente Marcos, C. Moni Bidin, S. Ortolani, G. Carraro, A&A **581**, A13 (2015)
- [11] B. Dias, B. Barbuy, I. Saviane, E.V. Held, G.S. Da Costa, S. Ortolani, M. Gullieuszik, M., S. Vasquez, A&A **590**, A9 (2016)
- [12] D. I. Dinescu, T.M. Girard, W. F. van Altena et al. et al. Astron. J. **125**, 1373 (2003)
- [13] D. I. Dinescu, T.M. Girard, W. F. van Altena et al. et al. Astron. J. **117**, 1792 (1999)
- [14] D. I. Dinescu, W. F. van Altena, T.M. Girard et al. Astron. J. **117**, 277 (1999)
- [15] D. I. Dinescu, T.M. Girard, W. F. van Altena, et al. Astron. J. **114**, 1014 (1997)
- [16] S. Feltzing and R.A. Johnson Astron. and Astrophys. **385**, 67 (2002)
- [17] T. K. Fritz, N. Kallivayalil Astrophys. J. **811**, 123 (2015)
- [18] Gaia Collaboration et al. Astron. and Astrophys. **595**, 1 (2016)
- [19] M. Miyamoto, R. Nagai, Astronomical Society of Japan, **27**, no. 4, 533, (1975)
- [20] L. Hernquist, Astron. J. , **356**, 359, (1990)
- [21] A. S. Rastorguev et al. Astrophysical Bulletin, **72**, issue 2, 122, (2017)
- [22] G. de Vaucouleurs, K. C. Freeman Vistas in Astronomy, **14**, issue 1, 163, (1972)
- [23] W.E. Harris, Astron. J. **112**, 1487 (1996) (2010 edition)
- [24] N. V. Kharchenko, A. E. Piskunov, S. Roeser, E. Schilbach, R. D. Scholz Astron. and Astrophys. **558**, 53 (2013)
- [25] A. D.Klinichev, E. V. Glushkova, A. K. Dambis, and L. N. Yalyalieva, Astron. Rep. (2018), in press.
- [26] A. Koch, C.J. Hansen, A. Kunder, A&A **604**, A41 (2017)
- [27] A.H.W. Küpper, E. Balbinot, A. Bonaca et al. Astrophys. J. **803**, 80 (2015)
- [28] A. Mainzer, T. Grav, J. Bauer et al. Astrophys. J. **743**, 156 (2011)
- [29] S.R. Majewski and K.M. Cudworth Publ. Astron. Soc. Pacific **105**, 987 (1993)
- [30] D. Massari, A. Bellini, F. R. Ferraro et al. Astrophys. J. , **779**, 81 (2013)
- [31] D. Michalik, L. Lindegren, and D. Hobbs, Astron. and Astrophys. , **574**, 115 (2015)
- [32] D.G. Monet, S.E. Levine, B. Canzian, et al. Astron. J. **125**, 984 (2003)
- [33] L.J. Rossi, S. Ortolani, B. Barbuy, et al. Monthly Notices Royal Astron. Soc. **450**, 3270 (2015)
- [34] R. Sch"onrich, J. Binney, W. Dehnen, MNRAS **403**, 1829 (2010)
- [35] M.F. Skrutskie, R.M. Cutri, R. Stiening, et al. Astron. J. **131**, 1163 (2006)
- [36] M. B. Taylor, Astronomical Society of the Pacific Conference Series **351**, 666 (2006)
- [37] J.-J. Wang, L. Chen, and D. Chen Astron. and Astrophys. , **29**, 386 (2005)
- [38] L.L. Watkins and R.P. van der Marel Astrophys. J. **839**, 89, (2017)
- [39] E.L. Wright, P.R.M. Eisenhardt, A.K. Mainzer, et al. Astron. J. **140**, 1868 (2010)
- [40] N. Zacharias, C. Finch, and J. Flouard Astron. J. **153**, 166 (2017)
- [41] N. Zacharias, C. Finch, J. Subasavage, et al., AJ **150**, 101 (2015)
- [42] M. Zoccali, A. Renzini, S. Ortolani, et al. Astron. J. **121**, 2638 (2001)